VIP Supercapacitors Very Important Paper

DOI: 10.1002/anie.201407836

Ultrahigh Energy Density Realized by a Single-Layer β-$Co(OH)_2$ All-Solid-State Asymmetric Supercapacitor**

Shan Gao, Yongfu Sun, Fengcai Lei, Liang Liang, Jiawei Liu, Wentuan Bi, Bicai Pan, and Yi Xie**

Abstract: *A conceptually new all-solid-state asymmetric supercapacitor based on atomically thin sheets is presented which offers the opportunity to optimize supercapacitor properties on an atomic level. As a prototype, β-$Co(OH)_2$ single layers with five-atoms layer thickness were synthesized through an oriented-attachment strategy. The increased density-of-states and 100 % exposed hydrogen atoms endow the β-$Co(OH)_2$ single-layers-based electrode with a large capacitance of 2028 $F g^{-1}$. The corresponding all-solid-state asymmetric supercapacitor achieves a high cell voltage of 1.8 V and an exceptional energy density of 98.9 $Wh kg^{-1}$ at an ultrahigh power density of 17981 $W kg^{-1}$. Also, this integrated nanodevice exhibits excellent cyclability with 93.2 % capacitance retention after 10000 cycles, holding great promise for constructing high-energy storage nanodevices.*

The current energy demand has greatly stimulated research on developing new electrode materials for advanced energy-storage devices.[1] In this regard, supercapacitors have received considerable attention as high-performance energy storage devices since they can provide superior capacitance, high power density, and long cycle life.[2] However, the commercially available capacitors usually suffer from an inferior energy density, which is lower than that of lead-acid batteries, Ni metal hydride (Ni-MH) batteries, or lithium-ion batteries.[3] Hence, fabricating a supercapacitor that can store as much energy as the lithium-ion batteries will be considered as a breaktrough in the field of energy technology.

Generally, improvement of energy density (E) can be achieved by maximizing the cell voltage (V) and the specific capacitance (C) according to Equation (1):

$$E = 0.5\,C\,V^2 \quad (1)$$

To improve the cell voltage, a promising strategy is to develop an all-solid-state asymmetric supercapacitor consisting of a battery-type Faradaic electrode and a capacitor-type electrode. Such a device has the potential to provide a maximum operation voltage up to 2.0 V and hence greatly improve the energy density. On the other hand, to improve the specific capacitance, various materials, such as metal hydroxides, have been widely investigated as cathodes in asymmetric supercapacitors.[4] Among them, β-$Co(OH)_2$ is one of the most promising candidates owing to its high theoretical capacitance of 3460 $F g^{-1}$ and natural abundance.[5a] However, the capacitances of β-$Co(OH)_2$-based pseudocapacitors are still much lower than their theoretical value.[5] This is mainly ascribed to the poor electrical conductivity and insufficient amount of electroactive sites in the previously prepared β-$Co(OH)_2$ samples, which lead to sluggish electrode kinetics and low specific capacitances.[6] Thus, it is desirable to fabricate a novel cathode material with abundant active sites and increased conductivity.

Herein, a conceptually new all-solid-state asymmetric supercapacitor based on atomically thin sheets is presented, offering increased specific capacitance and cell voltage, and hence increased energy density. The β-$Co(OH)_2$ material consisting of five-atom layers not only features a shorter ion diffusion path but also provides 100 % exposed hydrogen

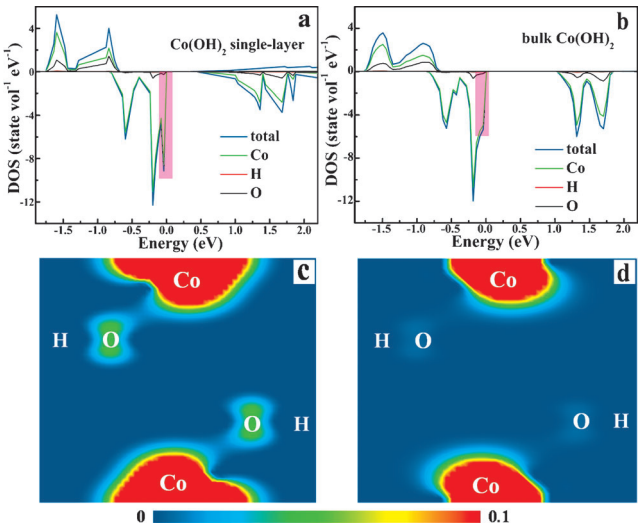

Figure 1. a,b) Calculated density-of-states for a) β-$Co(OH)_2$ single-layers and b) bulk β-$Co(OH)_2$. The shadowed region highlights the increased states density at the valence band edge of the β-$Co(OH)_2$ single-layers. c,d) Charge density waves for the valence band maximum of c) β-$Co(OH)_2$ single-layers and d) bulk β-$Co(OH)_2$, plotted from 0 (blue) to 0.1 $eÅ^{-3}$ (red).

[*] S. Gao, Dr. Y. Sun, F. Lei, L. Liang, J. Liu, W. Bi, Prof. B. Pan, Prof. Y. Xie
Hefei National Laboratory for Physical Sciences at Microscale, University of Science & Technology of China
Hefei, Anhui 230026 (P.R. China)
E-mail: yfsun@ustc.edu.cn
yxie@ustc.edu.cn

[**] This work was financially supported by the National Natural Science Foundation (21331005, 21422107, 11079004, 21201157, 11321503), the Chinese Academy of Science (XDB01020300), and the Program for New Century Excellent Talents in University (NCET-13-0546).

Supporting information for this article (experimental details, characterization, and electrochemical measurements) is available on the WWW under http://dx.doi.org/10.1002/anie.201407836.

atoms to serve as the electroactive sites, thus favoring Faradaic redox reactions, and hence achieving large storage capacitance and fast rate capability.[7] In addition, our systematic studies reveal that the atomically thin sheets possess much increased density-of-states (DOS) near the Fermi level as compared to their bulk counterparts, which could enhance their electrical conductivity.[7a,d] The calculated DOS in Figure 1 a,b clearly reveals that the β-$Co(OH)_2$ single-layers display remarkably increased states density at the valence band edge relative to the bulk material. This is further confirmed by the corresponding charge density wave in Figure 1 c,d. The increased DOS facilitates electrons transport along the two-dimensional conducting channels to react with OH^- ions, thus achieving fast diffusion kinetics.[7d]

Here, a simple room-temperature 2D oriented attachment approach is proposed to realize the first large-scale synthesis of β-$Co(OH)_2$ single-layers with five-atom thickness (Scheme S1 in the Supporting Information, SI). The XRD pattern in Figure 2 a can be readily indexed to brucite-like β-$Co(OH)_2$ (JCPDS No. 74-1057),[8] with the exclusive presence of the (00l) diffraction peaks. This reasonably reveals the preferred (001) orientation, in fair agreement with the HRTEM and fast-Fourier transform image in Figure 2 e,f. Moreover, the XPS spectra in Figure S2a–c indicate that the as-prepared products consist of the elements Co and O, indicating the formation of pure β-$Co(OH)_2$. This is further verified by the corresponding Raman spectrum and FT-IR spectrum in Figure S2d and Figure S3. In addition, the nearly transparent appearance of the nanosheets and the distinct Tyndall phenomenon in Figure 2 b clearly show the ultrathin and flexible nature of the obtained products. The AFM image and corresponding height profiles in Figure 2 c,d depict smooth 2D nanosheets with an average height of 0.47 nm, which is consistent with the 0.46 nm thickness of a single-layered β-$Co(OH)_2$ slab along the *c*-axis direction (inset in Figure 2 a and Figure S1), confirming the formation of β-$Co(OH)_2$ single-layers with five-atom thickness. The above results clearly demonstrate that clean β-$Co(OH)_2$ single-layers with five-atom thickness were successfully synthesized.

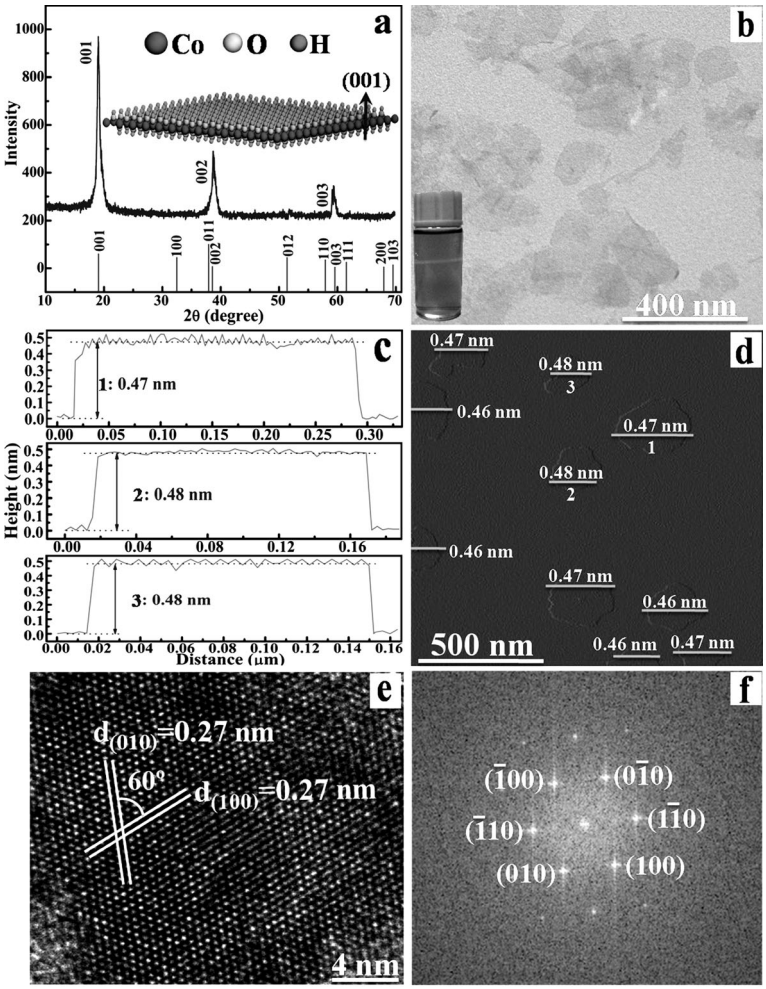

Figure 2. a) XRD pattern of a single-layer β-$Co(OH)_2$ film fabricated by a layer-by-layer assembly strategy; the inset shows the corresponding crystal structure in (001) orientation. b) Transmission electron microscopy (TEM) image of single-layer β-$Co(OH)_2$ and colloidal ethanol dispersion displaying the Tyndall effect. c) Height profiles derived from the atomic force microscopy (AFM) image in (d). The numbers 1 to 3 in (c) correspond to 1 to 3 in (d). e) High-resolution TEM (HRTEM) and f) the corresponding fast-Fourier transform image.

To explore the formation mechanism of the flexible β-$Co(OH)_2$ single-layers, time-dependent morphology evolution experiments were carried out by HRTEM. In an initial stage, part of aminoethanol hydrolyzes to produce NH_3^+-$(CH_2)_2OH$ and OH^- ions.[9] After the injection of aminoethanol solution into the $CoCl_2$ solution, the OH^- ions enable the Co^{2+} to form many small 2D β-$Co(OH)_2$ seeds without obvious orientation (Figure 3 a). $NH_3^+(CH_2)_2OH$ tends to adsorb on the (001) facet of the β-$Co(OH)_2$ seeds to further reduce the surface energy,[10] owing to the fact that the low surface energy renders the (001) facet much more stable than the (100) and (010) facets with high surface energy (Figure 3 e,f). The presence of $NH_3^+(CH_2)_2OH$ confers the (001) facet with a positive charge. Driven by electrostatic interactions and hydrogen-bond interactions between the NH_3^+-$(CH_2)_2OH$ adsorbents,[11] the small seeds organize into nanosheets through an oriented attachment process. A close inspection of Figure 3 b identifies that three small 2D seeds merge into one nanosheet, indicating that the nanosheets are formed directly from the small 2D β-$Co(OH)_2$ seeds by oriented attachment.[12] As the oriented attachment process continues, the small 2D nanosheets ultimately evolve into large 2D nanosheets (Figure 3 c,d). After 36 h, the distinct interplanar *d*-spacing of 0.27 nm matches well with the {100} lattice plane of hexagonal β-$Co(OH)_2$, evidencing that β-$Co(OH)_2$ single-layers with exposed (001) planes were prepared (Figure 2 b,e and f). Therefore, the combination of crystal anisotropy and surfactant effects plays an important role in the formation of the flexible β-$Co(OH)_2$ single-layers.

A structural analysis of the obtained hexagonal β-$Co(OH)_2$ shows that the five-atom thickness enables the β-

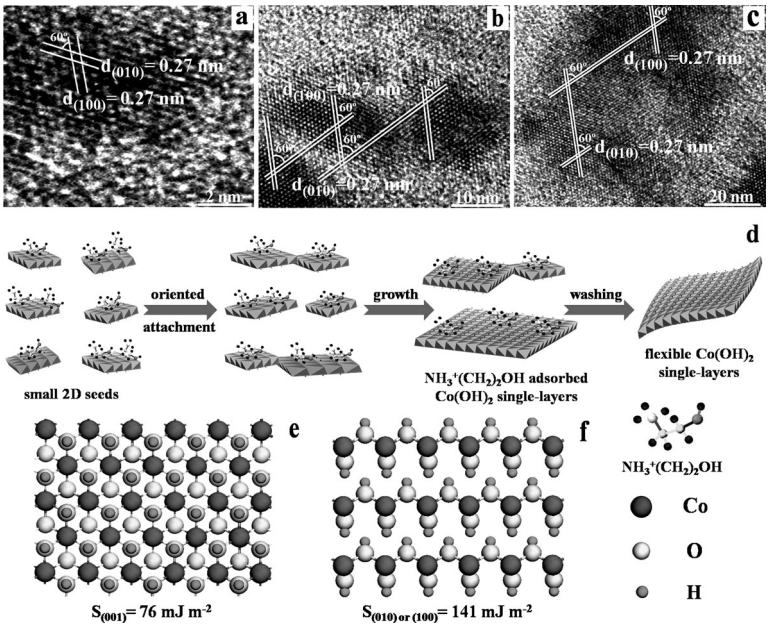

Figure 3. HRTEM images of the intermediate products at different reaction stages: a) 5 h; b) 10 h; c) 18 h. d) Schematic of the 2D oriented attachment strategy for the formation of the flexible β-$Co(OH)_2$ single-layers. e) Planar (001) facet and f) lateral (100) or (010) facets of hexagonal β-$Co(OH)_2$ showing calculated surface energies of 76 and 141 mJ m^{-2}.

$Co(OH)_2$ single-layer to expose all hydrogen atoms on its surface. As shown in Figure S6, the single-layer β-$Co(OH)_2$ electrode shows a high specific capacitance of 2028 F g^{-1} compared with the 7 nm thick nanosheet β-$Co(OH)_2$ (998 F g^{-1}) and bulk β-$Co(OH)_2$ plate electrodes (525 F g^{-1}). An all-solid-state asymmetric supercapacitor was fabricated consisting of our single-layer β-$Co(OH)_2$ cathode and an N-doped graphene-based anode.[13] As shown in Figure 4a, the cyclic voltammetry (CV) curves of the single-layer β-$Co(OH)_2$ all-solid-state asymmetric supercapacitor exhibit rectangular shapes even at a high scan rate of 100 mV s^{-1}, indicating ideal capacitive behavior and fast charge/discharge properties.[14b,15] The typical charge–discharge curves in Figure 4b show a nearly linear variation with potential, proving its capacitor-like behavior.[14d] The specific capacitances calculated from the galvanostatic charge–discharge curves are 241.9, 236.3, 231.8, 225.7, and 219.6 F g^{-1} at current density of 1, 2, 5, 10, and 20 A g^{-1}, respectively (Figure 4b). This specific capacitance of the integrated asymmetric supercapacitor is comparable to the 251.3 F g^{-1} of the N-doped graphene-based electrode in Figure S7b, further demonstrating the high capacitance of the single-layer β-$Co(OH)_2$ electrode.

High specific capacitance and large cell voltage are crucial to realize a high-efficiency supercapacitor with high energy density and high power density based on the Equation (1) as well as Equation (2):[14b]

$$P = E/\Delta t \quad (2)$$

where E, P, and Δt are the specific energy density (Wh kg^{-1}), power density (kW kg^{-1}), and discharge time (s), respectively.

Figure 4c shows the Ragone plots of our single-layer β-$Co(OH)_2$ all-solid-state asymmetric supercapacitor in the voltage window of 0–1.8 V at various current densities. The specific energy density decreased from 108.9 to 98.9 Wh kg^{-1} based on the total mass of active materials, while the power density increased from 0.9 to 17.98 kW kg^{-1} as the current density increased from 1 to 20 A g^{-1}. To the best of our knowledge, such an energy density of 98.9 Wh kg^{-1} and power density of 17.981 kW kg^{-1} at high current density of 20 A g^{-1} for an integrated asymmetric supercapacitor can compete with the world's highest energy density for supercapacitors (Figure 4c).[14] Also, a high energy density of 43.9 Wh kg^{-1} could be obtained for the integrated asymmetric supercapacitor based on the total mass of the integrated nanodevice (73.6 mg), which is still comparable with Ni-MH batteries.[3] Moreover, its capacitance was 93.2% of the initial capacitance at a scan rate of 20 mV s^{-1} after 10000 cycles (Figure 4d), indicating an excellent cycling stability, which could be further proved by the corresponding CV curves in the inset of Figure 4d. Such cycling performance is highly competitive in comparison with some other asymmetric supercapacitors.[14b–f,16]

Obviously, the ultrahigh energy density of the single-layer β-$Co(OH)_2$ all-solid-state asymmetric supercapacitor can be ascribed to the elevated cell voltage of 1.8 V and high specific capacity of 241.9 F g^{-1}, according to formula (1). The presence of the single-layer β-$Co(OH)_2$ cathode and N-doped graphene-based anode helps to greatly extend the cell voltage of the integrated device up to 1.8 V, thus drastically improving the energy density. Also, the specific capacitance of the full device is significantly enhanced by the ultrahigh specific capacity of 2025 F g^{-1} of the single-layer β-$Co(OH)_2$ cathode (Figure S8a). The perfect specific capacitance of the β-$Co(OH)_2$ single-layer can be assigned to its ultrathin thickness and the 100% exposed hydrogen atoms. It was reported that the charge/discharge process of β-$Co(OH)_2$ is a quasi-adsorption/desorption process of surface hydrogen atoms,[5b] implying that an architecture with more exposed hydrogen atoms would favor the electrochemical redox reactions. The five-atom thickness of our β-$Co(OH)_2$ single-layers enable 100% hydrogen atom exposure on the surface (Figure 4e). Compared with bulk β-$Co(OH)_2$ plates and 7 nm thick β-$Co(OH)_2$ nanosheets (Figures S4 and S5), the 100% exposed hydrogen atoms of the β-$Co(OH)_2$ single-layers provide much more chance for hydrogen desorption and hence efficiently facilitate the Faradaic redox reactions according to reactions (3) and (4):

$$Co(OH)_2 + OH^- \rightleftharpoons CoOOH + H_2O + e^- \quad (3)$$

$$CoOOH + OH^- \rightleftharpoons CoO_2 + H_2O + e^- \quad (4)$$

which contribute to higher capacitance and superior rate capability.[1b,17] Also, the huge specific surface area provides

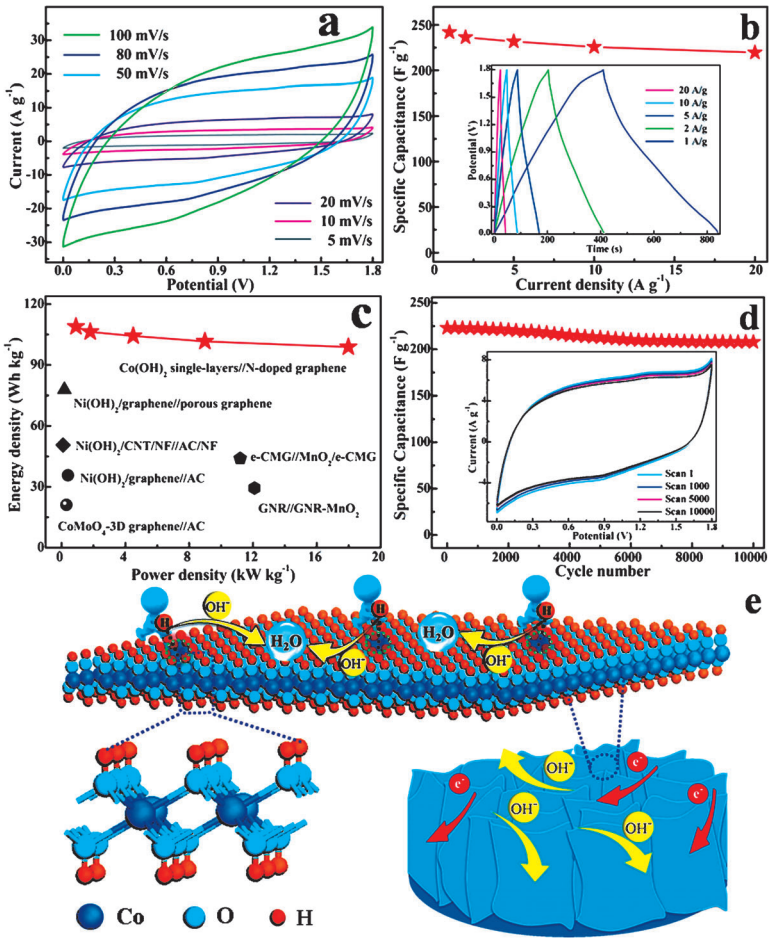

Figure 4. a) CV curves at various scan rates and b) galvanostatic charge–discharge curves at different current densities (inset) and the corresponding calculated specific capacitances of the single-layer β-$Co(OH)_2$ all-solid-state asymmetric supercapacitor. c) Electrochemical performance of the single-layer β-$Co(OH)_2$ all-solid-state asymmetric supercapacitor in comparison with previously reported asymmetric supercapacitors. d) Cycle performance of the single-layer β-$Co(OH)_2$ all-solid-state asymmetric supercapacitor measured at a scan rate of 20 $mV s^{-1}$; the inset shows the corresponding CV curves. e) Schematic illustration of the hydrogen adsorption/desorption process in the single-layer β-$Co(OH)_2$ electrode.

an enlarged electrolyte-accessible area, while the ultrathin thickness facilitates diffusion of the electrolyte ions at the high rates. The excellent electrochemical kinetics are further shown by the increased specific current compared with the 7 nm thick β-$Co(OH)_2$ nanosheets and the bulk β-$Co(OH)_2$ plates electrodes (Figure S6a).[7c,18] Moreover, the enhanced DOS of the β-$Co(OH)_2$ single-layers (Figure 1) facilitates electron transport along the two-dimensional conducting channels to react with OH^- ions, which is favorable for fast diffusion kinetics.[7d,17b] Also, the 2D configuration endows the β-$Co(OH)_2$ single-layers with a much better grain boundary connectivity and intimate contact with the electrolyte, thus ensuring fast interfacial charge transfer and fast electrochemical reactions as well as low corrosion rates.[7d,12] This could be verified by their lower resistance of ca. 1.0 Ω in the high-frequency region and their steeper slope in the low-frequency region of the Nyquist plot, compared to that of the 7 nm β-$Co(OH)_2$ nanosheets and the bulk β-$Co(OH)_2$ plates electrodes in Figure S9.[1b,7c] Accordingly, the above several advantages endow the single-layer β-$Co(OH)_2$ electrode with prominently improved specific capacitance and faster electrode kinetics, thus providing an ideal platform for the fabrication of asymmetric supercapacitors with a wider voltage range and hence higher energy density.

In summary, a conceptually new all-solid-state asymmetric supercapacitor based on an atomically thin-sheet electrode was described, showing high energy density due to abundant active sites and increased electrical conductivity. As a prototype, large-scale flexible β-$Co(OH)_2$ single-layers with five-atom thickness were synthesized through a facile oriented attachment method. The five-atom thickness and 100% exposed hydrogen atoms facilitate the hydrogen desorption process, while the increased DOS at the valence band edge favors electron transport along the 2D conducting channels. These advantages enable the single-layer β-$Co(OH)_2$ electrode to achieve excellent electrochemical kinetics and perfect capacitance of 2028 $F g^{-1}$. Benefiting from these features, an all-solid-state asymmetric supercapacitor fabricated from single-layer β-$Co(OH)_2$ displayed a high energy density of 98.9 $Wh kg^{-1}$ at an exceptional power density of 17981 $W kg^{-1}$, which is comparable to that of lithium-ion batteries. Furthermore, this integrated asymmetric supercapacitor achieves excellent cycling life, with 93.2% capacity retention after 10000 charge/discharge cycles.

Received: August 1, 2014
Published online: September 22, 2014

Keywords: all-solid-state devices · asymmetric supercapacitors · energy materials · oriented attachment · thin films

[1] a) J. R. Miller, P. Simon, *Science* **2008**, *321*, 651; b) C. Z. Yuan, J. Y. Li, L. R. Hou, X. G. Zhang, L. F. Shen, X. W. Lou, *Adv. Funct. Mater.* **2012**, *22*, 4592; c) Q. Lu, J. G. Chen, J. Q. Xiao, *Angew. Chem. Int. Ed.* **2013**, *52*, 1882; *Angew. Chem.* **2013**, *125*, 1932.

[2] M. R. Lukatskaya, O. Mashtalir, C. E. Ren, Y. Dall'Agnese, P. Rozier, P. L. Taberna, M. Naguib, P. Simon, M. W. Barsoum, Y. Gogotsi, *Science* **2013**, *341*, 1502.

[3] a) X. W. Yang, C. Cheng, Y. F. Wang, L. Qiu, D. Li, *Science* **2013**, *341*, 534; b) C. G. Liu, Z. N. Yu, D. Neff, A. Zhamu, B. Z. Jang, *Nano Lett.* **2010**, *10*, 4863; c) Y. Gogotsi, P. Simon, *Science* **2011**, *334*, 917.

[4] a) C. Z. Yuan, L. Yang, L. R. Hou, L. F. Shen, X. G. Zhang, X. W. Lou, *Energy Environ. Sci.* **2012**, *5*, 7883; b) P. Simon, Y. Gogotsi, *Nat. Mater.* **2008**, *7*, 845.

[5] a) C. Z. Yuan, X. G. Zhang, L. R. Hou, L. F. Shen, D. K. Li, F. Zhang, C. G. Fan, J. M. Li, *J. Mater. Chem.* **2010**, *20*, 10809; b) B. G. Choi, M. H. Yang, S. C. Jung, K. G. Lee, J. G. Kim, H. S. Park, T. J. Park, S. B. Lee, Y. K. Han, Y. S. Huh, *ACS Nano* **2013**, *7*, 2453; c) T. Wu, C. Z. Yuan, *Mater. Lett.* **2012**, *85*, 161; d) L. Cao, F. Xu, Y. Y. Liang, H. L. Li, *Adv. Mater.* **2004**, *16*, 1853.

[6] L. Huang, D. C. Chen, Y. Ding, S. Feng, Z. L. Wang, M. L. Liu, *Nano Lett.* **2013**, *13*, 3135.
[7] a) Y. F. Sun, Z. H. Sun, S. Gao, H. Cheng, Q. H. Liu, J. Y. Piao, T. Yao, C. Z. Wu, S. L. Hu, S. Q. Wei, Y. Xie, *Nat. Commun.* **2012**, *3*, 1057; b) Q. Li, B. D. Guo, J. G. Yu, J. R. Ran, B. H. Zhang, H. J. Yan, J. R. Gong, *J. Am. Chem. Soc.* **2011**, *133*, 10878; c) H. L. Wang, Z. W. Xu, A. Kohandehghan, Z. Li, K. Cui, X. H. Tan, T. J. Stephenson, C. K. King'ondu, C. M. B. Holt, B. C. Olsen, J. K. Tak, D. Harfield, A. O. Anyia, D. Mitlin, *ACS Nano* **2013**, *7*, 5131; d) Y. F. Sun, H. Cheng, S. Gao, Q. H. Liu, Z. H. Sun, C. Xiao, C. Z. Wu, S. Q. Wei, Y. Xie, *J. Am. Chem. Soc.* **2012**, *134*, 20294.
[8] Z. P. Liu, R. Z. Ma, M. Osada, K. Takada, T. Sasaki, *J. Am. Chem. Soc.* **2005**, *127*, 13869.
[9] L. Sun, R. Shao, Z. D. Chen, L. Q. Tang, Y. Dai, J. F. Ding, *Appl. Surf. Sci.* **2012**, *258*, 5455.
[10] J. T. Jang, S. Jeong, J. W. Seo, M. C. Kim, E. Sim, Y. Oh, S. Nam, B. Park, J. Cheon, *J. Am. Chem. Soc.* **2011**, *133*, 7636.
[11] a) Z. L. Zhang, Z. Y. Tang, N. A. Kotov, S. C. Glotzer, *Nano Lett.* **2007**, *7*, 1670; b) Z. Y. Tang, Z. L. Zhang, Y. Wang, S. C. Glotzer, N. A. Kotov, *Science* **2006**, *314*, 274.
[12] C. Schliehe, B. H. Juarez, M. Pelletier, S. Jander, D. Greshnykh, M. Nagel, A. Meyer, S. Foerster, A. Kornowski, C. Klinke, H. Weller, *Science* **2010**, *329*, 550.
[13] Y. Zhao, C. G. Hu, Y. Hu, H. H. Cheng, G. Q. Shi, L. T. Qu, *Angew. Chem. Int. Ed.* **2012**, *51*, 11371; *Angew. Chem.* **2012**, *124*, 11533.
[14] a) X. Z. Yu, B. G. Lu, Z. Xu, *Adv. Mater.* **2014**, *26*, 1044; b) J. Yan, Z. J. Fan, W. Sun, G. Q. Ning, T. Wei, Q. Zhang, R. F. Zhang, L. J. Zhi, F. Wei, *Adv. Funct. Mater.* **2012**, *22*, 2632; c) M. K. Liu, W. W. Tjiu, J. S. Pan, C. Zhang, W. Gao, T. X. Liu, *Nanoscale* **2014**, *6*, 4233; d) Z. Tang, C. h. Tang, H. Gong, *Adv. Funct. Mater.* **2012**, *22*, 1272; e) H. B. Li, M. H. Yu, F. X. Wang, P. Liu, Y. Liang, J. Xiao, C. X. Wang, Y. X. Tong, G. W. Yang, *Nat. Commun.* **2013**, *4*, 1894; f) B. G. Choi, M. H. Yang, W. H. Hong, J. W. Choi, Y. S. Huh, *ACS Nano* **2012**, *6*, 4020.
[15] Z. J. Fan, J. Yan, T. Wei, L. J. Zhi, G. P. Ning, T. Y. Li, F. Wei, *Adv. Funct. Mater.* **2011**, *21*, 2366.
[16] L. B. Kong, M. Liu, J. W. Lang, Y. C. Luo, L. Kang, *J. Electrochem. Soc.* **2009**, *156*, A1000.
[17] a) F. Jiao, H. Frei, *Angew. Chem. Int. Ed.* **2009**, *48*, 1841; *Angew. Chem.* **2009**, *121*, 1873; b) Y. F. Sun, Q. H. Liu, S. Gao, H. Cheng, F. C. Lei, Z. H. Sun, Y. Jiang, H. B. Su, S. Q. Wei, Y. Xie, *Nat. Commun.* **2013**, *4*, 2899.
[18] a) H. Li, J. Wu, Z. Y. Yin, H. Zhang, *Acc. Chem. Res.* **2014**, *47*, 1067; b) X. Huang, C. L. Tan, Z. Y. Yin, H. Zhang, *Adv. Mater.* **2014**, *26*, 2185; c) X. Huang, Z. Y. Zeng, H. Zhang, *Chem. Soc. Rev.* **2013**, *42*, 1934; d) X. Huang, X. Y. Qi, F. Boey, H. Zhang, *Chem. Soc. Rev.* **2012**, *41*, 666.

